RESEARCH BRIEF

Biallelic Alteration and Dysregulation of the Hippo Pathway in Mucinous Tubular and Spindle Cell Carcinoma of the Kidney

Rohit Mehra[1,2,3], Pankaj Vats[1,3,4], Marcin Cieslik[3], Xuhong Cao[3,5], Fengyun Su[3], Sudhanshu Shukla[3], Aaron M. Udager[1], Rui Wang[3], Jincheng Pan[6], Katayoon Kasaian[3], Robert Lonigro[3], Javed Siddiqui[3], Kumpati Premkumar[4], Ganesh Palapattu[7], Alon Weizer[2,7], Khaled S. Hafez[7], J. Stuart Wolf Jr[7], Ankur R. Sangoi[8], Kiril Trpkov[9], Adeboye O. Osunkoya[10], Ming Zhou[11], Giovanna A. Giannico[12], Jesse K. McKenney[13], Saravana M. Dhanasekaran[1,3], and Arul M. Chinnaiyan[1,2,3,5,7]

ABSTRACT Mucinous tubular and spindle cell carcinoma (MTSCC) is a relatively rare subtype of renal cell carcinoma (RCC) with distinctive morphologic and cytogenetic features. Here, we carry out whole-exome and transcriptome sequencing of a multi-institutional cohort of MTSCC ($n = 22$). We demonstrate the presence of either biallelic loss of Hippo pathway tumor suppressor genes (TSG) and/or evidence of alteration of Hippo pathway genes in 85% of samples. *PTPN14* (31%) and *NF2* (22%) were the most commonly implicated Hippo pathway genes, whereas other genes such as *SAV1* and *HIPK2* were also involved in a mutually exclusive fashion. Mutations in the context of recurrent chromosomal losses amounted to biallelic alterations in these TSGs. As a readout of Hippo pathway inactivation, a majority of cases (90%) exhibited increased nuclear YAP1 protein expression. Taken together, nearly all cases of MTSCC exhibit some evidence of Hippo pathway dysregulation.

SIGNIFICANCE: MTSCC is a rare and relatively recently described subtype of RCC. Next-generation sequencing of a multi-institutional MTSCC cohort revealed recurrent chromosomal losses and somatic mutations in the Hippo signaling pathway genes leading to potential YAP1 activation. In virtually all cases of MTSCC, there was evidence of Hippo pathway dysregulation, suggesting a common mechanistic basis for this disease. *Cancer Discov; 6(11); 1258–66. ©2016 AACR.*

INTRODUCTION

Several large-scale sequencing studies have sought to understand the biology of the most common renal cell carcinomas (RCC), including the clear-cell [kidney renal clear-cell carcinoma (KIRC); ref. 1], papillary [kidney renal papillary cell carcinoma (KIRP); ref. 2], and chromophobe [kidney chromophobe (KICH); ref. 3] subtypes; however, rarer subtypes of RCC have not been characterized comprehensively at the genomic level. Mucinous tubular and spindle cell

[1]Department of Pathology, University of Michigan Health System, Ann Arbor, Michigan. [2]Comprehensive Cancer Center, University of Michigan Health System, Ann Arbor, Michigan. [3]Michigan Center for Translational Pathology, Ann Arbor, Michigan. [4]Department of Biomedical Science, School of Basic Medical Sciences, Bharathidasan University, Tiruchirappalli, Tamil Nadu, India. [5]Howard Hughes Medical Institute, Ann Arbor, Michigan. [6]Department of Urology, First Affiliated Hospital, Sun-Yat Sen University, Guangzhou, China. [7]Department of Urology, University of Michigan Health System, Ann Arbor, Michigan. [8]El Camino Hospital, Department of Pathology, Mountain View, California. [9]Department of Pathology and Laboratory Medicine, University of Calgary, Calgary, Alberta, Canada. [10]Departments of Pathology and Urology, Emory University School of Medicine, Atlanta, Georgia. [11]Department of Pathology, New York University School of Medicine, New York, New York. [12]Departments of Pathology, Microbiology, and Immunology, Vanderbilt University School of Medicine, Nashville, Tennessee. [13]Cleveland Clinic, Robert J. Tomsich Pathology and Laboratory Medicine Institute, Cleveland, Ohio.

Note: Supplementary data for this article are available at Cancer Discovery Online (http://cancerdiscovery.aacrjournals.org/).

R. Mehra, P. Vats, and M. Cieslik contributed equally to this article.

S.M. Dhanasekaran and A.M. Chinnaiyan share senior authorship of this article.

Corresponding Author: Arul M. Chinnaiyan, University of Michigan, 1400 East Medical Center Drive, 5316 CCGC 5940, Ann Arbor, MI 48109-5940. Phone: 734-615-4062; Fax: 734-615-4055; E-mail: arul@umich.edu

doi: 10.1158/2159-8290.CD-16-0267

carcinoma (MTSCC) is a relatively rare, recently characterized, but well-established subtype of RCC that contains a biphasic epithelioid and spindle cell component (4). Although the majority of patients with these tumors have a favorable prognosis, a small but distinct subset can be associated with an aggressive clinical phenotype and poor outcome.

MTSCC demonstrates a relatively consistent immunophenotype, cytogenetic aberration pattern, and express lineage-specific markers of the kidney, such as PAX8 (5). These characteristics, combined with the unique morphologic phenotype of MTSCC (a variable combination of epithelial spindle cells with focal to abundant stromal mucin), suggest that this tumor may have a convergent mechanism of pathogenesis. To explore this, we assembled a multi-institutional cohort of 22 MTSCCs and carried out whole-exome sequencing of tumor matched with adjacent normal samples, as well as capture transcriptome sequencing of the samples (6). This integrative sequencing strategy allowed us to broadly survey single-nucleotide variations (SNV), small insertions–deletions (indels), germline alterations, amplifications and deletions, gene fusions, and expression signatures (7, 8).

RESULTS

Mutational Landscape and Recurrent Hippo Pathway Mutations in MTSCC

The mean patient age in our MTSCC cohort was 62 years (range, 44–78 years), with a variable tumor size (mean, 5.1 cm; range, 2.0–15.0 cm; Supplementary Table S1). All 22 tumors exhibited classic morphologic features of MTSCC, as described above and illustrated in Fig. 1A (confirmed by two genitourinary pathologists, J.K. McKenney and R. Mehra). We obtained genomic DNA from matched tumor and normal formalin-fixed paraffin-embedded (FFPE) tissue samples and analyzed them by whole-exome sequencing (see Methods). Capture transcriptome libraries were generated from total RNA isolated from matched tumor and normal samples (Methods). We obtained high-quality exome sequencing data from all 22 tumor/normal samples as indicated by the high alignment, depth of coverage, and overall low PCR duplication rate (Supplementary Table S2). In addition, we also obtained high-quality capture transcriptome data implied by the high spliced junctions (indicative of transcriptome library complexity) from 10 matched tumor–normal specimens (Supplementary Table S2). Analysis of matched tumor/normal capture genome data revealed a relatively low number of somatic mutations within the coding region in both the discovery ($n = 10$) and validation ($n = 12$) cohorts. MTSCC exhibited an average of 9 nonsynonymous mutation calls per sample, ranging from 2 to 26. MTSCC contains an average of 0.86 mutations per Mb, which is (Fig. 1B) consistent with previously reported low mutation rates in kidney cancers of 1.45, 1.1, and 0.4 mutations per Mb in KIRC (1), KIRP (2), and KICH (3), respectively, excluding samples with a hypermutator phenotype characteristic of defective DNA mismatch repair. The somatic mutation data were queried for trinucleotide signature patterns reported by Alexandrov and colleagues (9), but no significant pattern was noted, primarily due to the low mutation burden in this disease (data not shown).

To identify mutations with likely functional significance, somatic calls were ranked according to known activating oncogenic mutations and recurrent inactivating tumor suppressor mutations (Supplementary Table S3). This classification aided in the immediate recognition of highly recurrent Hippo pathway tumor suppressor gene (TSG) mutations in our list. This included recurrent somatic alterations in the protein tyrosine phosphatase nonreceptor type 14 (*PTPN14*) in 7 cases (7/22, 31%) with a median variant allele frequency (VAF) of 66%, neurofibromin-2 (*NF2*; merlin) in 5 cases (5/22, 23%) at 58% median VAF, besides salvador homolog 1 (*SAV1*) and Itchy E3 Ubiquitin Protein Ligase (*ITCH*; ref. 10) in 1 case each with 77% and 39% VAF, respectively (Supplementary Table S3). All *PTPN14*, *NF2*, and *SAV1* mutations observed were loss-of-function resulting from either frameshift insertions/deletions (indels; 7 cases), splice-site mutations (5 cases), or nonsense mutation (1 case). Schramm and colleagues (11) recently reported two relapsed neuroblastoma cases with loss-of-function missense mutations in *PTPN14* and showed that ectopic expression of the mutant PTPN14 (T42A) protein increased clonogenic growth in the SK-N-SH cell line. Hence, PTPN14's functionality in binding and negatively regulating YAP1 oncogenic function (12) may be compromised in our index cases. *NF2*, an extensively studied tumor suppressor gene, is an upstream regulator of the Hippo pathway, and its mutation results in nonmalignant brain tumors in a syndrome termed neurofibromatosis type 2 (13). Although *SAV1* is a core member of the Hippo pathway, most of the mutated genes in this cohort are established associate members (14). SAV1 is known to interact with the MST1 kinase and enhance Large Tumor Suppressor Kinase (*LATS*) phosphorylation, which in turn negatively regulates YAP (13). Hence, losses in *NF2*, *SAV1*, and *PTPN14* in MTSCC will likely result in YAP1 activation in the corresponding index tumors.

We also observed additional somatic mutations in independent cases among established members such as Dachsous Cadherin-Related 2 (*DCHS2*) and Homeodomain Interacting Protein Kinase 2 (*HIPK2*) and putative Hippo pathway genes involving Zinc Finger DHHC-Type Containing 5 (*ZDHHC5*) and Zinc Finger DHHC-Type Containing 15 (*ZDHHC15*; ref. 15; Supplementary Table S3). However, aberrations in *HIPK2*, *DCHS2*, *ZDHHC5*, and *ZDHHC15* aberrations may all represent subclonal events, as the *VAF*s of 16%, 4%, 10%, and 21%, respectively, are lower compared with the other Hippo pathway calls (Supplementary Table S3). To study this further, we obtained exome sequencing data from three independent tumor sites that are spatially well separated, from 3 cases, namely, RC_1099, RC_1098, and RC_1097 (Supplementary Fig. S1). In RC_1099, all sites sequenced showed high VAF for *PTPN14* mutation, demonstrating its clonal nature. As expected, in both RC_1098 and RC_1097, the VAFs for *DCHS2* substantially increased in two independent sites and were absent in the third, whereas the VAF for *ZDHHC5* showed significant increase in one another site, supporting the subclonal nature of these aberrations (Supplementary Fig. S1).

Recurrent Copy-Number Alterations and Biallelic Loss of Hippo Pathway Tumor Suppressor Genes in MTSCC

Owing to widespread chromosomal loss commonly observed in MTSCC, we reasoned that a second hit, particularly in TSGs,

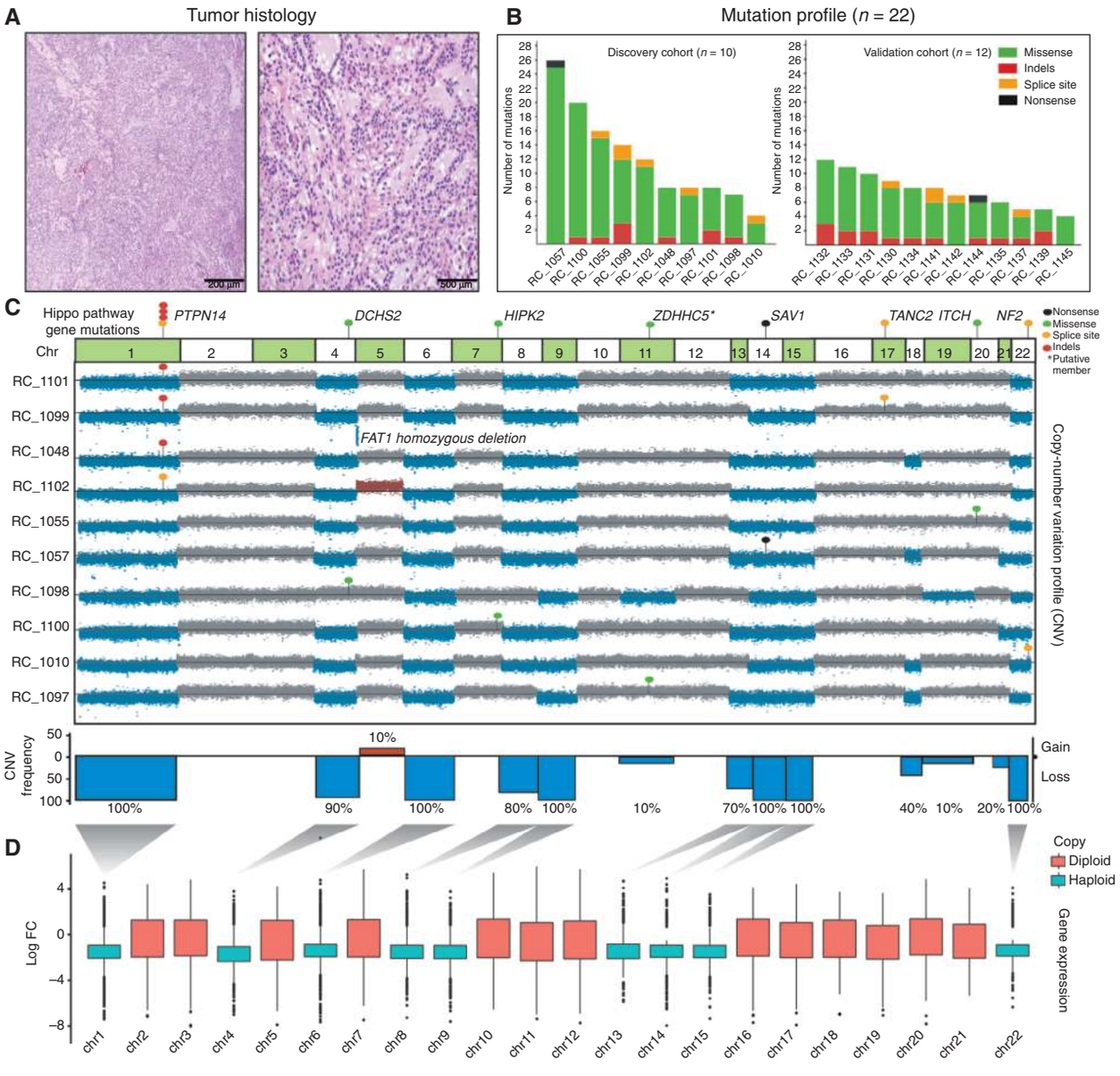

Figure 1. Integrative analysis of genomic alterations in MTSCC. **A,** representative microscopic images of MTSCC cases that were sequenced. Low magnification, 40× (left; scale bar, 200 μm) and high magnification, 200× (right; scale bar, 500 μm). **B,** histogram representing the total number of nonsynonymous somatic mutations identified in each sample in the discovery cohort ($n = 10$; left) and the validation cohort ($n = 12$; right). **C,** integrated view of the frequencies of chromosomal aneuploidy and Hippo pathway gene mutations identified in the MTSCC discovery cohort ($n = 10$). Chromosomes with copy loss (blue) and gain (red) are indicated. Indels (red dots), missense SNVs (green dots), nonsense (black dots), and splice-site SNVs (yellow dots) in *PTNP14, DCHS2, HIPK2, SAV1, TANC2, ITCH,* and *NF2* genes are indicated. *TANC2* and *ITCH* are recently nominated putative Hippo pathway regulators that require additional experimental validation. **D,** global reduction of transcript levels due to chromosomal copy loss. Shown is the distribution of fold changes for all significantly differentially expressed loci per chromosome (chromosomes with copy loss: blue; diploid: red) in the RNA-sequencing data from the discovery cohort ($n = 4$ tumor/normal pairs).

may be acquired via copy-number variation (CNV). To investigate this, we generated copy-number profiles (Methods) from matched tumor/normal capture genome data and queried for recurrent events in this disease. Our analysis of the 22 cases revealed monosomy of chromosomes 1, 6, 9, 14, 15, and 22 in 100% of cases, and chromosomes 4, 8, and 13 with 90%, 81%, and 90%, respectively (Fig. 1C; Supplementary Fig. S2A). Importantly, chromosomes 1, 14, and 22 harbor *PTPN14*, *SAV1*, and *NF2* genes, respectively, and showed one copy loss in all samples, which amounts to biallelic loss of these Hippo pathway TSGs in the index tumors. The recurrent chromosomal loss we observed by exome sequencing supports a recent study by Peckova and colleagues (16) that reported similar recurrent chromosomal losses using array CGH and FISH strategies. Importantly, none of the samples in this cohort with pure MTSCC histology displayed chromosomes 7 and 17 gains, commonly noted as gains

in type I papillary RCC (17). The recent papillary RCC (KIRP) study by The Cancer Genome Atlas (TCGA) Research Network reported Hippo pathway mutations (*NF2* and *SAV1*) in 4% of the samples and used CNV to classify tumors into 3 groups, such as genome stable, unstable, and chromosome 7/17 gains (2). Given the morphologic overlap between MTSCC and a minor subset of papillary RCC (PRCC), we used our knowledge of mutations and copy-number patterns to identify any possibly misclassified samples in the TCGA KIRP cohort (2). We first investigated the level 3 TCGA copy-number data available for 161 KIRP cases by principal component analysis and observed at least 3 outlier samples (TCGA-B3-3926, TCGA-F9-A7QO, and TCGA-UN-AAZ9), with the signature MTSCC type chromosomal losses and lacking characteristic genetic alterations associated with type I PRCC (ref. 2; Supplementary Fig. S2B and S2C), and subsequent analysis of the updated TCGA KIRP cohort ($n = 288$) identified a fourth case (TCGA-G7-A8LC). Interestingly, *SAV1* loss-of-function mutations combined with a haploid status of chromosome 14 observed in the 3 cases suggested a double hit in this Hippo pathway gene. The fourth sample had a missense mutation in *DOCK11*, which could be a potential Hippo pathway regulator located on the X chromosome, similar to roles proposed for DOCK7, 8, and 9 recently (refs. 18 and 19; Supplementary Fig. S2C). Our analysis of the TCGA KIRP data showed that Hippo pathway mutations are frequently associated with genome-unstable KIRP samples with various cancer subtype classifications (mutually exclusive of chr17/7 gain and *MET* mutations; Supplementary Fig. S2D).

Besides the chromosome level losses observed in our current study, we also observed few focal copy losses such as FAT Tumor Suppressor Homolog 1 (*FAT1*) loss in RC_1099. We also observed rare gains of whole chromosome 5 (2/22 cases); however, focal gains were absent. Taken together, integration of somatic mutation and copy-number data revealed homozygous loss of the critical Hippo pathway tumor suppressor genes (*PTPN14*, *SAV1*, and *NF2*) as a recurrent molecular theme in MTSCC. Importantly, we noticed that most cases in this cohort had strong evidence for mutually exclusive aberration in at least one Hippo pathway gene [except RC_1099, and RC_1139, where we saw additional aberrations among potential Hippo pathway members, namely, *TANC2*, *SKIV2L2* (refs. 19–21) mutations, and *FAT1* loss; Fig. 1C].

MTSCC Gene Expression Analysis

To assess whether the pattern of chromosomal loss is reflected at the transcriptome level, we examined the RNA-sequencing (RNA-seq) data obtained in the discovery cohort from four matched tumor–normal pairs generated in this study. Upon identifying loci (genes and intergenic regions) with significant differential expression, we found that on the haploid chromosomes the great majority of loci showed a global decrease in transcript levels relative to the diploid chromosomes (Fig. 1D). This link is further accentuated in the Gviz plot, which shows a gene-wise representation where a vast majority of the genes on haploid chromosomes (1, 4, 6, 8, 9, 13, 14, 15 and 22) showed decreased expression as compared with diploid chromosomes (2, 3, 5, 7, 10, 11, 12, 16, 17, 18, 19, 20, 21; Supplementary Fig. S3A). Overall, the majority of differentially expressed genes in MTSCC were downregulated (Supplementary Fig. S3B). To identify transcriptional targets of the Hippo pathway in the kidney, we performed *PTPN14* knockdown followed by RNA-seq in two kidney cancer cell lines (CAKI-1 and A-704) and a normal kidney epithelial cell line (HK-2). *PTPN14* siRNAs were first functionally validated in an MCF-7 TEAD reporter luciferase stable cell line. Both siRNAs showed comparable knockdown efficiency and significantly increased luciferase reporter activity (Supplementary Fig. S4A and data not shown). In two of the kidney cell lines, *PTPN14* knockdown increased cell proliferation compared with nontarget controls (Supplementary Figs. S4B and S4C). Although we observed excellent correlation between genes dysregulated by either *PTPN14* or *LATS1* knockdown within each cell line (HK2, CAKI-1, and A704; Supplementary Fig. S4D), the overlap across the three cell lines was only 23 genes (Supplementary Figs. S4E and Supplementary Table S4). Further, these 23 genes did not show concordant differential expression in MTSCC tumors (Supplementary Fig. S4F). Overall, these results illustrate the marked tissue specificity of Hippo pathway targets.

In an alternate approach to assess the functional impact of Hippo pathway inactivation, we performed enrichment analysis and identified several altered transcriptional signatures. We noted enrichment of hepatocyte nuclear factor (HNF) targets where HNF4A/1A targets were significantly downregulated (Supplementary Fig. S5A and Supplementary Table S5). *HNF1* and *HNF4* are master regulators of the hepatic transcriptome and considered tumor suppressor genes in liver cancer. Interestingly, a recent study has directly implicated the Hippo pathway in regulating hepatocyte differentiation where enhancer occupancy of HNF4A and FOXA2 was modulated by YAP activation (22). In addition, another previous report showed downregulation of *HNF4A*, upregulation of *HNF1B* upon ectopic YAP overexpression in mouse liver organoids (ref. 23; Supplementary Fig. S5B). Because hepatocyte nuclear factors are drivers of kidney development and differentiation (24, 25), they may also play a role in the ubiquitous downregulation of kidney marker expression observed in MTSCC (Supplementary Fig. S5C). In the normal human tissue RNA-seq compendia data from The Genotype Tissue Expression study (GTEX data; ref. 26), significant HNF gene expression was found in liver, colon, pancreas, kidneys, and small intestine (Supplementary Fig. S6A), and in the kidney, prominent HNF expression was noted in renal proximal tubules (27, 28). We next assessed *HNF1A*, *HNF1B*, and *HNF4A* transcript expression in MTSCC and the TCGA pan–kidney cancer data set (1–3; Supplementary Figs. S6B and S6C). We found that among major renal cancers, chromophobe RCC (KICH) showed the most significant downregulation of *HNF1A* and *HNF4A* similar to MTSCC, which suggests that loss of HNF transcriptional activity is common across renal cancers, as previously reported (ref. 29; Supplementary Figs. S6D and S6E).

YAP1 Protein Expression in MTSCC

The deleterious somatic mutations in the *PTPN14*, *NF2*, and *SAV1* genes in the context of their functional protein domains are depicted in Fig. 2A. Loss of function of negative regulators of the Hippo pathway, such as the kinases *LATS* and Serine/Threonine Kinase 4 (*STK4*, also called *MST*), and factors such as *NF2* and *PTPN14* are known to stabilize the transcription coactivator protein YAP1 and increase its nuclear localization

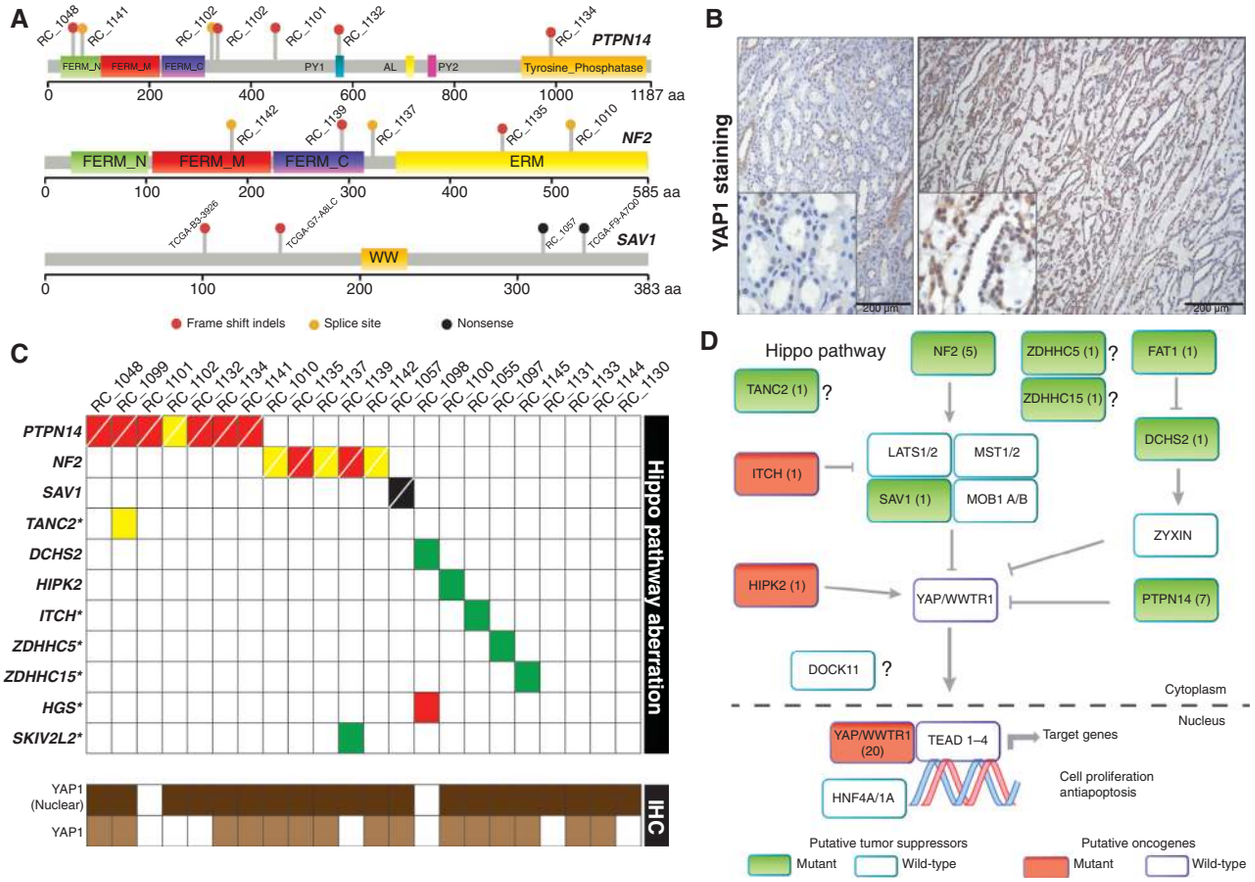

Figure 2. Hippo pathway gene alterations in MTSCC. **A,** schematic representation of the Hippo pathway gene aberrations discovered in MTSCC. PFAM domains and scale depicting amino acid (aa) numbers are presented for each protein schema. Indels (red dots), nonsense SNVs (black dots), and splice-site SNVs (yellow dots). **B,** an example of YAP1 nuclear expression in MTSCC case RC_1100 as revealed by IHC. Benign background renal parenchyma (left; low-power view 100× with scale bar 200 μm, and inset 400×) demonstrates patchy and weak predominantly nuclear YAP1 staining (with focal cytoplasmic expression). Tumor areas of MTSCC (right; low-power view 100× with scale bar 200 μm, and inset 400×) from the same case demonstrate moderate to strong nuclear YAP1 expression (with focal cytoplasmic staining). **C,** MTSCC Hippo pathway mutations in the cohort (top; red, indels; yellow, splice site; black, nonsense; green, missense; cells crossed with white line indicate biallelic loss; asterisks indicate putative members) represented along with case-wise evaluation of YAP1 protein nuclear localization (bottom; dark brown, present; white, absent) and increased YAP1 protein expression in tumor compared with background benign renal parenchyma (bottom; light brown, present; white, absent). **D,** Hippo signaling pathway schematic with alterations identified in this study is highlighted. Pathway members with mutations are indicated (filled boxes) and numbers within represent the cases with that particular somatic aberration (except in the nuclear YAP1 box where the numbers represent IHC staining data for cases with nuclear localization); putative tumor suppressors are colored green and oncogenes are colored red; question marks indicate uncharacterized putative members.

(11, 13, 23). In addition, our cell line experiments demonstrated upregulation of YAP transcriptional activity in an established reporter cell line and increased cell proliferation upon PTPN14 knockdown in various kidney cell lines (Supplementary Fig. S4). Nuclear localization of YAP1 will render support to Hippo pathway inactivation caused by loss of the tumor suppressors *PTPN14*, *NF2*, and *SAV1*. Immunohistochemistry (IHC) assessment with a validated anti-YAP1 antibody revealed YAP1 protein nuclear localization in 90% of the MTSCC tumors (Fig. 2B and C; Supplementary Fig. S7A and S7B and Supplementary Table S6). Among the 13 tumors with biallelic loss of hippo pathway tumor suppressors (NF2, SAV1, and PTPN14), all samples showed nuclear YAP staining except one where the staining was very weak (Fig. 2C). In addition, we also noticed increased YAP1 protein expression in tumors compared with background benign renal parenchyma in 68% of cases (Fig. 2B and 2C; Supplementary Fig. S7A and S7B and Supplementary Table S6). In comparison, concurrent YAP1 IHC performed on a tissue microarray (TMA) consisting of 21 clear-cell RCCs, 21 papillary RCCs, 22 chromophobe RCCs, 22 oncocytomas, and 10 benign renal tissues demonstrated these cases to be negative for YAP1 overexpression (Supplementary Table S6). Taken together, the Hippo pathway alterations in MTSCC predominantly consist of loss-of-function events in putative tumor suppressor components and missense aberrations in putative oncogenic components, likely leading to oncogenic YAP1 activation (Fig. 2D). When genetic alteration of the Hippo pathway is considered along with nuclear YAP1 protein expression, nearly all cases evaluated exhibited some evidence of Hippo pathway dysregulation, suggesting a convergent mechanism of pathogenesis.

Putative Cellular Origin of MTSCC

To identify nephron sections that could potentially give rise to MTSCC, we followed correlation-based approaches as proposed by Davis and colleagues for KICH (3). We leveraged two existing data sets of human (30) and rat (31) dissected nephrons obtained through serial analysis of gene expression (SAGE) and RNA-seq, respectively. To emphasize differences in gene expression patterns that are specific to MTSCC and the various nephron sections, all expression profiles were standardized relative to normal kidney tissue (see Methods). We also identified marker genes specifically expressed in each rat nephron section. An outline of the analyses is represented in Supplementary Fig. S8A. Correlations were calculated across either all genes (Supplementary Fig. S8B), all marker genes (n = 600; Supplementary Fig. S8C and S8D), or specific transcription factors (n = 41; see Methods). As expected, strong correlations with proximal tubule, terminal portions of the proximal tubule, and distal nephron sections were noted for TCGA KIRC, KIRP, and KICH, respectively. MTSCC samples showed substantial heterogeneity, but appeared distinct from all other major RCC types. Overall, a trend of positive correlations was observed for some sections of the proximal tubule and loop of Henle, whereas mostly negative correlations were observed for distal nephron regions for both human and rat data sets (Supplementary Fig. S8B, S8D, and S8E). To further discriminate between MTSCC and KICH, the two types of RCC with an overlapping pattern of chromosome losses, we restricted the correlation analysis to transcription factors, previously shown to exhibit cell-type specificity across nephron sections (31). Interestingly, MTSCC samples positively correlated with the loop of Henle, a region that was previously speculated to be associated with MTSCC (32), whereas conversely KICH strongly correlated with distal tubule (ref. 3; Supplementary Fig. S8F). For example, *IRX5*, a marker of loop of Henle, is highly expressed in MTSCC and absent in KICH, whereas *FOXI1*, a marker of the distal nephron, was present in KICH and absent in MTSCC (Supplementary Fig. S8G).

DISCUSSION

Our study now adds MTSCC to a growing list of cancers (13) with recurrent aberrations among Hippo pathway members, including somatic mutations, gene fusions, and copy-number variations. Unlike the basal cell carcinomas involving the skin, which harbor a high mutational burden and where the loss of Hippo pathway genes *LATS1* and *PTPN14* was observed in 31% of cancers (33), recurrent Hippo pathway aberrations with a low overall mutational burden (Fig. 1B) and recurrent chromosomal losses (Fig. 1C) seem to define the molecular signature of MTSCC. The current study provides evidence for the first time about the existence of intratumor mutational heterogeneity in MTSCC. Distinct chromosomal copy-number variations are a recurring theme in RCCs such as KICH (3) with losses in chromosomes 1, 2, 6, 10, 13, and 17; KIRP (2) with gains in chromosomes 7 and 17; and MTSCC. We believe further subgrouping of renal cancer samples profiled thus far, based on variation in a CNV pattern, may identify novel disease subtypes that can then be refined by cross-platform integrative data analysis, which along with single-cell sequencing of normal kidney cell types and tumors may provide a deeper understanding of the ontology of these cancers.

The mechanisms and causes of these chromosomal losses, whether it is a sequential event and its association with tumor progression, remain an interesting and unanswered question. Chromosomal losses seem to have a major influence on the MTSCC gene expression pattern (Fig. 1D) and may likely alter Hippo pathway gene regulation in a disease- and tissue-specific manner. Our attempts to delineate Hippo pathway targets in the kidney by knockdown experiments showed very low overlap across the three different models, and genes such as *CTGF* and *CYR61*, previously shown to be induced by loss of the Hippo pathway in the liver, were not regulated in the kidney. These findings are consistent with the low overlap between YAP transcriptional targets identified in various profiling studies, indicating strong cell type– and tissue-specific gene regulation by the Hippo pathway (13). Lack of a cell line model for MTSCC hinders our efforts to further characterize the functional effects of Hippo pathway aberrations in this tumor. However, our analysis has identified several novel upregulated genes in MTSCC tumors, such as *VSTM2A* (Supplementary Fig. S3), both in our cohort and in TCGA index samples identified in Supplementary Fig. S2, which could be further evaluated as potential biomarkers.

Finally, the cell of origin for MTSCC remains controversial (16, 32, 34). Our results based on expression correlations with dissected nephron sections suggest loop of Henle as a putative candidate and support previous electron microscopic studies by Srigley and colleagues (32). Alternatively, MTSCC may arise from a rare cell type with low representation across the dissected nephron samples. Clearly, further studies are necessary to confirm these observations.

In summary, whole-exome and transcriptome sequencing of MTSCC revealed recurrent copy-number alterations and somatic mutations of Hippo signaling pathway genes. Biallelic loss of Hippo pathway tumor suppressor genes, namely *PTPN14*, *NF2*, and *SAV1*, was found in approximately 60% of MTSCCs (Fig. 2). Protein expression analysis by IHC further supported our model that implicates nuclear YAP1 (90%) and increased YAP protein levels (68%) in tumors, thus rendering further evidence of inactivation of the Hippo pathway in MTSCC. These data suggest that Hippo pathway dysregulation may be a fundamental causal event in the pathogenesis of MTSCC, a finding that may have diagnostic and therapeutic implications for this rare RCC subtype. Small-molecule inhibitors of YAP (a key downstream component of the Hippo pathway), such as verteporfin (13), present an attractive opportunity for targeted therapy in the rare patients with MTSCC with sarcomatoid differentiation or metastasis. These molecular data highlight the possibility of emerging clinical/therapeutic approaches to rare tumors in this era of precision oncology (35, 36).

METHODS

Sample Procurement and Clinical Study

Patient samples were procured from the University of Michigan Health System, Cleveland Clinic, Vanderbilt University, Emory School of Medicine, University of Calgary, and New York School of Medicine. This study was performed under Institutional Review Board–approved

protocols (with waiver of informed consent) and conducted in accordance with the principles of the Declaration of Helsinki. Tumor purity was assessed by study pathologists (R. Mehra and J. McKenney). Tumor and matched adjacent normal kidney sections were utilized to extract both genomic DNA and total RNA using an All Prep DNA/RNA FFPE kit. Sample details, including age, gender, and disease stage, are summarized in Supplementary Table S1.

Reagents

Anti-YAP1 antibody (catalog # 4912s) used for IHC and Western blot analysis was purchased from Cell Signaling Technology. *YAP1*, *PTPN14*, *LATS1*, and control siRNAs were purchased from either Thermofisher or Ambion.

Nucleic Acid Isolation

Genomic DNA and total RNA was isolated from five 10-μm sections of matched tumor and normal FFPE specimens using the All Prep FFPE DNA/RNA Isolation Kit (Qiagen). The gDNAs and total RNAs were quantitated using a Nanodrop spectrophotometer. RNA quality was determined using Bio-Analyzer.

Sequencing Library Preparation and Next-Generation Sequencing

Capture genome and capture transcriptome libraries were prepared as recently described with modifications (6, 37). Briefly, for capture genome libraries, 3 μg of gDNA was subjected to minimum shearing using Covaris. Libraries were prepared with Sciclone G3 NGS workstation (Perkin Elmer) following the Kappa HT library preparation kit protocol (Kappa Biosystems, catalog # KK8234) using the sheared DNA as input. Libraries were size-selected for 200 to 350 bp using dual SPRI bead selection and subjected to PCR amplification with KapaReadyMix reagent in the kit. One microgram of the library was used for capture with human all exon v4 capture probes following the manufacturer's instructions (Agilent). After hybridization and wash, the DNA bound to beads was PCR amplified, purified, and analyzed by BioAnalyzer before sequencing. For capture transcriptome libraries, 5 μg of total RNA was used in a reverse transcription reaction, and the obtained cDNA was subsequently taken to a second-strand DNA synthesis as described previously (6). Following second-strand synthesis, we used the Sciclone G3 NGS workstation (Perkin Elmer) with the Kappa HT library preparation kit to produce the libraries that were then captured with human all exon v4 capture probes as described above. Both capture genome and transcriptome libraries were sequenced using HiSeq 2500 (Illumina) as described in ref. 6. All data sets will be deposited in the public repository Database of Genotypes and Phenotypes (dbGaP) upon acceptance for publication.

Western Blotting

Half a million H1299 cells were plated in 6-well plates the day before transfection. YAP1 or control siRNAs (silencer select) were transfected with RNAiMax (Thermofisher), and 48 hours after transfection cells were lysed to monitor knockdown efficiency by Western blotting. For Western blotting, cell lysates were resolved in 4% to 12% NuPAGE gels and transferred onto nitrocellulose membranes. After transfer, the membrane was blocked in 5% milk and incubated with either anti-YAP1 (4°C overnight) or anti–GAPDH-HRP (1 hour, room temperature) antibodies. After washing, the YAP1 blot was incubated with HRP-conjugated secondary antibody, and the chemiluminescence signal was obtained with an ECL Kit (Amersham) and was captured on X-ray films.

Cell Lines, siRNA Transfection, Proliferation, RNA Isolation, and Quantitative Reverse Transcription PCR

CAKI-1, HK2, and A-704 cells were purchased from the ATCC in April 2015 and authenticated by STR DNA fingerprinting on June 30, 2015 (CAKI-1 and HK2), and August 20, 2015 (A-704), at the University of Michigan DNA Sequencing Core using Identifiler Plus kit (Applied Biosystems, Inc.), and the resulting amplicons were analyzed in the ABI3720XL Genetic Analyzer. Routine *Mycoplasma* testing was also performed using a MycoAlert Plus kit (Lonza) every 3 weeks while in culture, following manufacturer's recommendations. The cells were grown in McCoy, Keratinocyte, and RPMI media supplemented with 10% FBS, penicillin, and streptomycin, respectively. siRNAs were obtained from Ambion and transfected (25 nmol/L) using Lipofectamine RNAimax (Invitrogen). For transfection, 0.4 million cells were plated in a 6-well plate before transfection. Forty-eight hours after transfection, cells were trypsinized, counted, and replated for proliferation assay. Remaining cells were used for RNA isolation using a miRNA easy kit (Qiagen). RNA was converted to cDNA using Superscript III (Invitrogen) to perform qRT-PCR.

Luciferase Assay

MCF7 cells stably expressing TEAD-regulated luciferase were purchased (BPS Bioscience) and maintained in 10% DMEM supplemented with insulin. To study the effect of knockdown of PTPN14 on YAP1/TEAD-regulated luciferase, cells were transfected with 25 nmol/L of either nontargeting or *PTPN14* siRNAs. After 48 hours of transfection, cells were lysed in 1× passive lysis buffer (Promega). An equal amount of protein was used to measure the luciferase activity using luciferase assay reagent (Promega).

IHC

In the current study, IHC was performed on representative whole tumor sections from the MTSCC cases with anti-YAP1 primary antibody (Cell Signaling Technology; YAP1 Rabbit polyclonal catalog # 4912s; 1 in 300 dilution). Formalin-fixed paraffin sections were cut at 5 μm and rehydrated to water. Heat-induced epitope retrieval was performed with FLEX TRS Low pH Retrieval Buffer (6.1) for 20 minutes (Dako; FLEX TRS Low pH Retrieval Buffer, FLEX HRP EnVision Detection System). After peroxidase blocking, the antibody YAP1 rabbit polyclonal was applied at a dilution of 1:300 at room temperature for 60 minutes. The FLEX HRP EnVision System was used for detection. DAB chromagen was then applied for 10 minutes. Slides were counterstained with Harris Hematoxylin for 5 seconds, dehydrated, and coverslipped. IHC was assessed for nuclear and cytoplasmic expression on tumor cells and background benign renal parenchyma by two study pathologists (A.M. Udager and R. Mehra).

Data Analysis

Exome Analysis Whole-exome tumor/normal paired-end sequencing was performed on the Illumina HiSeq 2500 instrument, and base call files from the instrument were converted to fastq format using the Illumina cassava (8) pipeline. These fastq files were then aligned to human genome build 19 (GRCh37) using novoalign (version 2.08.02, Novocraft Technologies). The sorting and indexing of the bam files were carried out using novosort (1.02.01), and duplicate reads were removed using Picard (version 1.93); furthermore, using the Picard HsMetrics program, we estimated metrics such as on-target and mean coverage for all the libraries. SAMtools (version 0.1.19) was then used to generate the tumor/normal pileup files and were simultaneously used for mutation analysis using the VarScan 2 algorithm (version 2.3.5; refs. 38, 39). The somatic mutation vcf files generated were then post processed with variant having phred score > q20, with minimum requirement of at least 10× coverage in tumor library to consider a given position for mutation calling, and 10 unique variant reads were required in tumor libraries to make a call. The SNV vcf files were then annotated using annovar (02.01.16), and somatic mutations were further filtered out based on their frequency in 1000 Genomes (August 2015 release), the Single Nucleotide Polymorphism Database (dbSNP; version 142), and the

6500 Exome Sequencing Project. SNVs were also annotated with the Catalogue of Somatic Mutations in Cancer (COSMIC; version 70) and Clinvar for the hotspot/pathogenic mutations (40). Small insertion and deletion (indel) mutations were identified using Pindel (version 0.2.5). The candidate indels were further filtered by the homopolymer/repeat regions, recurrent sequencing artifacts, and high recurrence in 1000 Genomes, followed by manual curation and annotation using annovar (40). The variant allele fraction for indels presented in Supplementary Table S3 is based on independent estimation of allelic fractions from the BAM files.

Copy-number aberrations were quantified and reported for each gene as the segmented, normalized, $\log_2$-transformed exon coverage ratio between each tumor sample and its matched normal sample. To account for observed associations between coverage ratios and variation in guanine–cytosine content (GC) content across the genome, lowess normalization was used to correct per-exon coverage ratios before segmentation analysis. Specifically, mean GC percentage was computed for each targeted region, and a lowess curve was fit to the scatterplot of $\log_2$ coverage ratios versus mean GC content across the targeted exome using the lowess function in R (version 2.13.1) with smoothing parameter f = 0.05 (41).

RNA-seq Analysis Following sequencing and base calling, RNA-seq data were aligned using STAR (2.4.0g1; refs. 42, 43) to the GRCh38.p1 reference genome, using the "basic" version of gencode 22 to construct the splice junction database. To identify chromosome-level differences in gene expression, the genome was divided into genic and intergenic loci. The total number of reads mapping to each locus was counted using featureCounts (44). To correct for different sequencing depth and effective library size normalization factors, we applied the TMM function (default settings) on reads mapped to diploid chromosomes. Expression of protein-coding genes was quantified by counting the reads overlapping exons of annotated protein coding genes in strand-specific mode. Expression-level differences between tumor and normal samples were obtained by applying limma (45) with eBayes (46) adjustment on voom-transformed count data. Plots of locus-level expression were produced using GViz (47).

To compare MTSCC expression profiles with data sets from dissected nephrons, we followed a procedure analogous to that followed by Davis and colleagues (3) and Chen and colleagues (48). Briefly, MTSCC gene expression levels (RPKM) were standardized relative to the mean and standard deviation estimated from normal (benign) renal tissues combined across the KIRC, KIRP, and KICH TCGA cohorts. Similarly, expression levels (RPKM) from the rat dissected nephron RNA-seq data (31) were downloaded from GSE56743 and standardized relative to robust estimates of mean and standard deviation across the kidney sections. SAGE data from Cheval and colleagues (30) were centered and scaled as described previously (3). Concordance between expression profiles is reported as Pearson correlation. For human and rat comparisons only 1-to-1 orthologs are used, based on the mappings provided by Ensembl Genes 84. Region-specific markers for the rat data set were nominated as follows: For each region (n = 15), the top 40 genes with the most region-specific expression were found. Genes were ranked according to z-scores and sparsity (according to Hoyer; ref. 49) of expression within region. Further, highly correlated markers were removed (PCC > 0.95).

Gene-Set Enrichment Analysis (GSEA) Gene sets in the form of molecular signatures (MSigDb v5.0) and GO-term annotations have been downloaded from MSigDB and NCBI, correspondingly. All enrichment analyses have focused on protein-coding genes. Noncoding genes and genes without a mapping to Ensembl (sep2015.archive.ensembl.org) were removed from the signatures. The randomSet method (50) using shrunken fold changes from a gene-level score were used to identify significantly upregulated or downregulated signatures. RNA-seq data from siRNA experiments are deposited in Gene Expression Omnibus (GEO) under the accession number GSE85969.

Disclosure of Potential Conflicts of Interest

No potential conflicts of interest were disclosed.

Authors' Contributions

Conception and design: R. Mehra, P. Vats, G. Palapattu, K.S. Hafez, M. Zhou, S.M. Dhanasekaran, A.M. Chinnaiyan

Development of methodology: R. Mehra, P. Vats, M. Cieslik, X. Cao, F. Su, S. Shukla, S.M. Dhanasekaran, A.M. Chinnaiyan

Acquisition of data (provided animals, acquired and managed patients, provided facilities, etc.): R. Mehra, X. Cao, J. Pan, J. Siddiqui, A. Weizer, J.S. Wolf Jr, K. Trpkov, A.O. Osunkoya, M. Zhou, G.A. Giannico, J.K. McKenney, S.M. Dhanasekaran

Analysis and interpretation of data (e.g., statistical analysis, biostatistics, computational analysis): R. Mehra, P. Vats, M. Cieslik, S. Shukla, A.M. Udager, K. Kasaian, R. Lonigro, S.M. Dhanasekaran

Writing, review, and/or revision of the manuscript: R. Mehra, P. Vats, A.M. Udager, R. Wang, K. Premkumar, G. Palapattu, A. Weizer, K.S. Hafez, J.S. Wolf Jr, A.R. Sangoi, K. Trpkov, A.O. Osunkoya, M. Zhou, J.K. McKenney, S.M. Dhanasekaran, A.M. Chinnaiyan

Administrative, technical, or material support (i.e., reporting or organizing data, constructing databases): R. Mehra, P. Vats, X. Cao, F. Su, R. Wang, J. Siddiqui, J.K. McKenney

Study supervision: R. Mehra, A. Weizer, S.M. Dhanasekaran, A.M. Chinnaiyan

Acknowledgments

We thank Tina Fields, the histology staff, Lakshmi Dommeti, and Sunita Shankar for technical assistance; Rohit Malik for help with figures; Jyoti Athanikar and Chandan Kumar for manuscript editing; Terrance Barrette for computational infrastructure support; and Karen Giles for assistance with manuscript submission.

Grant Support

A.M. Chinnaiyan is supported by the A. Alfred Taubman Medical Institute, the American Cancer Society, the Howard Hughes Medical Institute, and EDRN U01 CA111275. R. Mehra and A.M. Chinnaiyan are supported by the Prostate Cancer Foundation and an UM1 grant (number 1UM1HG006508).

Received March 1, 2016; revised September 1, 2016; accepted September 2, 2016; published OnlineFirst September 7, 2016.

REFERENCES

1. Cancer Genome Atlas Research Network. Comprehensive molecular characterization of clear cell renal cell carcinoma. Nature 2013;499:43–9.
2. Linehan WM, Spellman PT, Ricketts CJ, Creighton CJ, Fei SS, Davis C, et al. Comprehensive molecular characterization of papillary renal-cell carcinoma. N Engl J Med 2016:135–45.
3. Davis CF, Ricketts CJ, Wang M, Yang L, Cherniack AD, Shen H, et al. The somatic genomic landscape of chromophobe renal cell carcinoma. Cancer Cell 2014;26:319–30.
4. Fine SW, Argani P, DeMarzo AM, Delahunt B, Sebo TJ, Reuter VE, et al. Expanding the histologic spectrum of mucinous tubular and spindle cell carcinoma of the kidney. Am J Surg Pathol 2006;30:1554–60.
5. Reuter VE, Argani P, Zhou M, Delahunt B, Members of the IIiDUPG. Best practices recommendations in the application of immunohistochemistry in the kidney tumors: report from the International Society of Urologic Pathology consensus conference. Am J Surg Pathol 2014;38:e35–49.
6. Cieslik M, Chugh R, Wu YM, Wu M, Brennan C, Lonigro R, et al. The use of exome capture RNA-seq for highly degraded RNA with application to clinical cancer sequencing. Genome Res 2015;25:1372–81.

7. Mody RJ, Wu YM, Lonigro RJ, Cao X, Roychowdhury S, Vats P, et al. Integrative clinical sequencing in the management of refractory or relapsed cancer in youth. Jama 2015;314:913–25.
8. Robinson DR, Wu YM, Vats P, Su F, Lonigro RJ, Cao X, et al. Activating ESR1 mutations in hormone-resistant metastatic breast cancer. Nat Genet 2013;45:1446–51.
9. Alexandrov LB, Nik-Zainal S, Wedge DC, Aparicio SA, Behjati S, Biankin AV, et al. Signatures of mutational processes in human cancer. Nature 2013;500:415–21.
10. Salah Z, Melino G, Aqeilan RI. Negative regulation of the Hippo pathway by E3 ubiquitin ligase ITCH is sufficient to promote tumorigenicity. Cancer Res 2011;71:2010–20.
11. Schramm A, Koster J, Assenov Y, Althoff K, Peifer M, Mahlow E, et al. Mutational dynamics between primary and relapse neuroblastomas. Nat Genet 2015;47:872–7.
12. Liu X, Yang N, Figel SA, Wilson KE, Morrison CD, Gelman IH, et al. PTPN14 interacts with and negatively regulates the oncogenic function of YAP. Oncogene 2013;32:1266–73.
13. Yu FX, Zhao B, Guan KL. Hippo pathway in organ size control, tissue homeostasis, and cancer. Cell 2015;163:811–28.
14. Harvey KF, Zhang X, Thomas DM. The Hippo pathway and human cancer. Nat Rev Cancer 2013;13:246–57.
15. Halder G, Johnson RL. Hippo signaling: growth control and beyond. Development 2011;138:9–22.
16. Peckova K, Martinek P, Sperga M, Montiel DP, Daum O, Rotterova P, et al. Mucinous spindle and tubular renal cell carcinoma: analysis of chromosomal aberration pattern of low-grade, high-grade, and overlapping morphologic variant with papillary renal cell carcinoma. Ann Diagn Pathol 2015;19:226–31.
17. Udager AM, Alva A, Mehra R. Current and proposed molecular diagnostics in a genitourinary service line laboratory at a tertiary clinical institution. Cancer J 2014;20:29–42.
18. Avruch J, Zhou D, Fitamant J, Bardeesy N, Mou F, Barrufet LR. Protein kinases of the Hippo pathway: regulation and substrates. Semin Cell Dev Biol 2012;23:770–84.
19. Moya IM, Halder G. Discovering the Hippo pathway protein-protein interactome. Cell Res 2014;24:137–8.
20. Couzens AL, Knight JD, Kean MJ, Teo G, Weiss A, Dunham WH, et al. Protein interaction network of the mammalian Hippo pathway reveals mechanisms of kinase-phosphatase interactions. Sci Signaling 2013;6:rs15.
21. Wang W, Li X, Huang J, Feng L, Dolinta KG, Chen J. Defining the protein–protein interaction network of the human hippo pathway. Mol Cell Proteomics 2014;13:119–31.
22. Alder O, Cullum R, Lee S, Kan AC, Wei W, Yi Y, et al. Hippo signaling influences HNF4A and FOXA2 enhancer switching during hepatocyte differentiation. Cell Rep 2014;9:261–71.
23. Yimlamai D, Christodoulou C, Galli GG, Yanger K, Pepe-Mooney B, Gurung B, et al. Hippo pathway activity influences liver cell fate. Cell 2014;157:1324–38.
24. Kanazawa T, Ichii O, Otsuka S, Namiki Y, Hashimoto Y, Kon Y. Hepatocyte nuclear factor 4 alpha is associated with mesenchymal–epithelial transition in developing kidneys of C57BL/6 mice. J Vet Med Sci 2011;73:601–7.
25. Kanazawa T, Konno A, Hashimoto Y, Kon Y. Hepatocyte nuclear factor 4 alpha is related to survival of the condensed mesenchyme in the developing mouse kidney. Dev Dyn 2010;239:1145–54.
26. Mele M, Ferreira PG, Reverter F, DeLuca DS, Monlong J, Sammeth M, et al. Human genomics. The human transcriptome across tissues and individuals. Science 2015;348:660–5.
27. Kanazawa T, Konno A, Hashimoto Y, Kon Y. Expression of hepatocyte nuclear factor 4alpha in developing mice. Anat Histol Embryol 2009;38:34–41.
28. Suh JM, Yu CT, Tang K, Tanaka T, Kodama T, Tsai MJ, et al. The expression profiles of nuclear receptors in the developing and adult kidney. Mol Endocrinol 2006;20:3412–20.
29. Saadettin S, Ebert T, Ryffel GU, Drewes T. Human renal cell carcinogensis is accompanied by a coordinate loss of the tissue specific transcription factors HNF4A and HNF1A. Cancer Lett 1996;101:205–10.
30. Cheval L, Pierrat F, Rajerison R, Piquemal D, Doucet A. Of mice and men: divergence of gene expression patterns in kidney. PloS One 2012;7:e46876.
31. Lee JW, Chou CL, Knepper MA. Deep sequencing in microdissected renal tubules identifies nephron segment-specific transcriptomes. J Am Soc Nephrol 2015;26:2669–77.
32. Srigley J, Kapusta L, Reuter V, Amin M, Grignon D, Eble J, et al. Phenotypic, molecular and utrastructural studies of a novel low grade renal epithelial neoplasm possibly related to the loop of Henle. Mod Pathol 2002;15.
33. Bonilla X, Parmentier L, King B, Bezrukov F, Kaya G, Zoete V, et al. Genomic analysis identifies new drivers and progression pathways in skin basal cell carcinoma. Nat Genet 2016;48:398–406.
34. Rakozy C, Schmahl GE, Bogner S, Storkel S. Low-grade tubular-mucinous renal neoplasms: morphologic, immunohistochemical, and genetic features. Mod Pathol 2002;15:1162–71.
35. Harms PW, Vats P, Verhaegen ME, Robinson DR, Wu YM, Dhanasekaran SM, et al. The distinctive mutational spectra of polyomavirus-negative Merkel cell carcinoma. Cancer Res 2015;75:3720–7.
36. Mehra R, Vats P, Kalyana-Sundaram S, Udager AM, Roh M, Alva A, et al. Primary urethral clear-cell adenocarcinoma: comprehensive analysis by surgical pathology, cytopathology, and next-generation sequencing. Am J Pathol 2014;184:584–91.
37. Robinson D, Van Allen EM, Wu YM, Schultz N, Lonigro RJ, Mosquera JM, et al. Integrative clinical genomics of advanced prostate cancer. Cell 2015;161:1215–28.
38. Koboldt DC, Zhang Q, Larson DE, Shen D, McLellan MD, Lin L, et al. VarScan 2: somatic mutation and copy number alteration discovery in cancer by exome sequencing. Genome Res 2012;22:568–76.
39. Li H, Handsaker B, Wysoker A, Fennell T, Ruan J, Homer N, et al. The sequence alignment/map format and SAMtools. Bioinformatics 2009;25:2078–9.
40. Wang K, Li M, Hakonarson H. ANNOVAR: functional annotation of genetic variants from high-throughput sequencing data. Nucleic Acids Res 2010;38:e164.
41. Lonigro RJ, Grasso CS, Robinson DR, Jing X, Wu YM, Cao X, et al. Detection of somatic copy number alterations in cancer using targeted exome capture sequencing. Neoplasia 2011;13:1019–25.
42. Dobin A, Davis CA, Schlesinger F, Drenkow J, Zaleski C, Jha S, et al. STAR: ultrafast universal RNA-seq aligner. Bioinformatics 2013;29:15–21.
43. Dobin A, Gingeras TR. Mapping RNA-seq reads with STAR. Current Protocols Bioinformat 2015;51:11 41–4 9.
44. Liao Y, Smyth GK, Shi W. The Subread aligner: fast, accurate and scalable read mapping by seed-and-vote. Nucleic Acids Res 2013;41:e108.
45. Ritchie ME, Phipson B, Wu D, Hu Y, Law CW, Shi W, et al. limma powers differential expression analyses for RNA-sequencing and microarray studies. Nucleic Acids Res 2015;43:e47.
46. Smyth GK. Linear models and empirical Bayes methods for assessing differential expression in microarray experiments. Stat Appl Genet Mol Biol 2004;3:Article3.
47. Law CW, Chen Y, Shi W, Smyth GK. voom: Precision weights unlock linear model analysis tools for RNA-seq read counts. Genome Biol 2014;15:R29.
48. Chen F, Zhang Y, Senbabaoglu Y, Ciriello G, Yang L, Reznik E, et al. Multilevel genomics-based taxonomy of renal cell carcinoma. Cell Rep 2016;14:2476–89.
49. Hoyer PO. Non-negative matrix factorization with sparseness constraints. J Mach Learning Res 2004;5:1457–69.
50. Newton MA. Random-set methods identify distinct aspects of the enrichment signal in gene-set analysis. Ann Appl Stat 2007:85–106.